Solar Energy Materials & Solar Cells 232 (2021) 111356

Contents lists available at ScienceDirect

Solar Energy Materials and Solar Cells

journal homepage: www.elsevier.com/locate/solmat

N-type polysilicon passivating contacts using ultra-thin PECVD silicon oxynitrides as the interfacial layer

Wenhao Chen [a,b,*], Josua Stuckelberger [b], Wenjie Wang [b,e], Sieu Pheng Phang [b], Daniel Macdonald [b], Yimao Wan [b,d], Di Yan [b,c,**]

[a] School of Testing and Photoelectric Engineering, Nanchang Hangkong University, Nanchang, 330063, China
[b] School of Engineering, The Australian National University, Canberra, ACT, 0200, Australia
[c] Department of Electrical and Electronic Engineering, University of Melbourne, Victoria, 3010, Australia
[d] Risen Energy Co., Ltd, Ningbo, 315609, China
[e] Key Laboratory of Artificial Structures and Quantum Control (Ministry of Education), Institute of Solar Energy School of Physics and Astronomy, Shanghai Jiao Tong University, Shanghai, 200240, China

ARTICLE INFO

Keywords:
Polysilicon passivating contacts
Silicon oxynitride
PECVD
Interfacial layers
Silicon solar cell

ABSTRACT

We describe the optimization of an ultra-thin silicon oxynitride (SiO_xN_y) layer deposited by plasma enhanced chemical vapor deposition (PECVD) as an interfacial layer for phosphorus doped polysilicon (poly-Si) passivating contacts. Our results demonstrate the possibility of depositing the thin interfacial layer and the intrinsic amorphous silicon (a-Si) film in a single PECVD process. We found that the gas flow rates strongly influence the properties of the SiO_xN_y layers, such as the refractive indices, chemical bond compositions and structural stabilities, which significantly affect the properties of the resulting polysilicon passivating contact structures. The passivation quality initially increased and then decreased with a decreasing N_2O/SiH_4 flow ratio, in the gas flow range of uniform deposition, while the contact resistivity decreased significantly. We found an optimal gas flow ratio of $N_2O:SiH_4:N_2 = 25:9:361$, with which we obtained uniform polysilicon passivating contacts with a high implied open-circuit voltage (iV_{oc}) of 711 mV and a low contact resistivity ρ_c of 6.6 mΩ cm^2.

1. Introduction

Contact structures using doped polysilicon (poly-Si) layers and thin dielectric films have been demonstrated as promising passivating contact structures in high efficiency silicon solar cells [1–5] with conversion efficiencies as high as 26% [6,7]. It has been shown that the ultrathin interfacial layer plays a critical role in the electrical performance of poly-Si passivating contacts [8,9]. The most common interfacial layer is silicon oxide (SiO_x) with a thickness of less than 2 nm, which can achieve both low recombination current densities of <5 fA/cm^2 and low contact resistivities of <10 mΩ cm^2 [10–12]. Such thin interfacial oxide layers can be formed in several ways that are generally separate from the silicon film deposition process, for example, hot nitric acid oxidation [13–15], high temperature thermal oxidation [16,17], ozone-based oxidation [18,19], etc. However, these processes require an additional step, and potentially increase the risk of contamination. Thus, fabrication schemes that integrate the growth of the interfacial SiO_x layers with the deposition of the polycrystalline or amorphous silicon layers have been investigated [20–23]. Additionally, introduction of N or other impurities in the interfacial layer can furtherly improve the electrical performance and thermal stability of the poly-Si passivating contact [21,24]. One study [25] has shown that the band gap of SiO_xN_y can be affected by changing the N/O ratio, which results in a change of the band bending and may affect the ability of carriers to tunnel through this SiO_xN_y layer [26]. Precise control and optimization of the chemical composition of such interfacial oxide layers may therefore help to improve their electrical properties. A controlled introduction of selected impurities to the interfacial oxide is challenging when using the conventional fabrication methods.

In this paper, we presented a single-side deposition process that combines the deposition of thin silicon oxynitride (SiO_xN_y) films and intrinsic amorphous silicon (a-Si) films in a single plasma enhanced chemical vapor deposition (PECVD) chamber. This offers a simple, fast and clean approach to fabricate poly-Si passivating contacts. At the same

* Corresponding author. School of Testing and Photoelectric Engineering, Nanchang Hangkong University, Nanchang, 330063, China.
** Corresponding author. School of Engineering, The Australian National University, Canberra, ACT, 0200, Australia.
E-mail addresses: whchen@nchu.edu.cn (W. Chen), di.yan@unimelb.edu.au (D. Yan).

https://doi.org/10.1016/j.solmat.2021.111356
Received 24 April 2021; Received in revised form 18 August 2021; Accepted 23 August 2021
Available online 27 August 2021
0927-0248/© 2021 Elsevier B.V. All rights reserved.

time, it allows us to manipulate the composition of the interfacial layer and its thickness. In this process, N is introduced into the interfacial layer using nitrous oxide (N_2O), silane (SiH_4) and nitrogen (N_2) as precursor gases [27–29] to deposit SiO_xN_y layers. The different chemical bond ratios of the interfacial layer can be adjusted by changing the gas flow rates. Furthermore, by using this PECVD deposition method, other impurities (e.g. C) could easily be introduced into the interfacial layer. Additionally, the deposition via PECVD has a faster growth rate (a thickness of ~2.2 nm was achieved within 10 s) compared to the conventional oxidation methods (i.e. a 1.4 nm SiO_x was formed in ~30 min by hot nitric acid oxidation [15,30]). In this work, firstly, we study the fundamental properties of the PECVD deposited SiO_xN_y layers, such as their growth rates, refractive index values, uniformities, and chemical bond compositions as a function of the precursor gas ratios. Subsequently, implementing these SiO_xN_y layers into n-type poly-Si passivating contacts using a similar doping approach to our previous studies [31,32], we study their electrical performance to obtain an optimal SiO_xN_y layer to achieve highly performing poly-Si contacts. The results indicate that small variations in the gas flow ratios can significantly change the atomic content of the interfacial layer, which affects the stability and electrical performance of the corresponding poly-Si passivating contacts.

2. Experimental methods

N-type commercial Czochralski (Cz) silicon wafers (1.3 Ω cm) with a thickness of ~180 μm were used both as passivation quality and contact resistivity test samples. The flowchart of experimental details is shown in Fig. 1. All samples were cleaned by standard RCA solutions, including both alkaline and acid based solutions, after a saw damage removal step. The SiO_xN_y/intrinsic a-Si stack was deposited at 400 °C by an inductively coupled PECVD system (Oxford Plasmalab 100, with N_2O, SiH_4 and N_2 as precursor gases for SiO_xN_y, and SiH_4 and He as precursor gases for a-Si). We adjusted the gas flow ratios over a wide range to ensure that the properties of the SiO_xN_y interfacial layer meet the requirements of passivating contact structure uniformity and thickness. After identifying the approximate range of optimal gas flows, five different SiO_xN_y layers

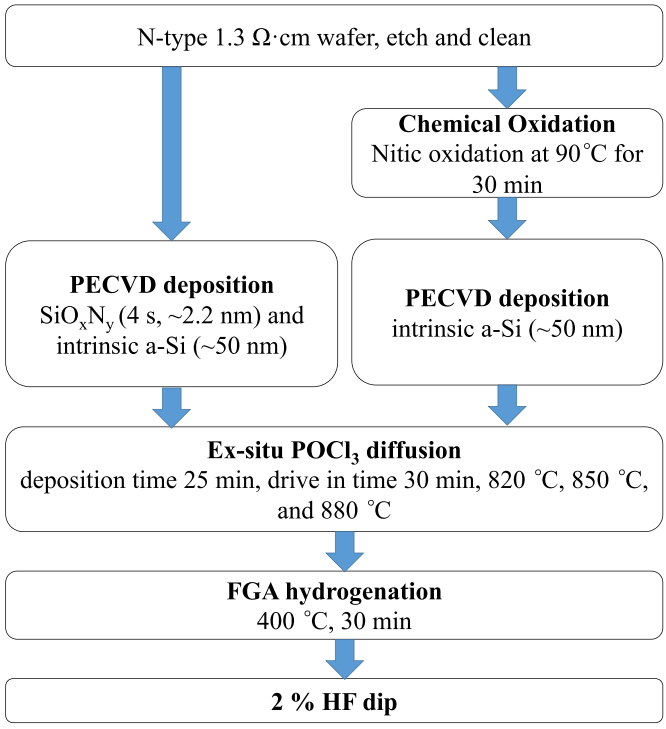

Fig. 1. Flowchart of experimental details.

were formed by modifying the gas flow ratio of N_2O and SiH_4 with values (in sccm) of 30:9, 25:9, 20:9, 20:11 and 20:13. The gas flow of N_2 remained constant at 361 sccm. The deposition time was fixed at 4 s. Subsequently, ~50 nm a-Si was deposited in the same chamber. The thickness and refractive index of different as-deposited SiO_xN_y films were measured by spectroscopic ellipsometry (JA Woollam M2000D). In addition, FTIR (Bruker VERTEX 80v) spectroscopy was used to study the SiO_xN_y film composition. A group of samples with an interfacial SiO_x prepared chemically by immersing in (68 wt%) nitric acid at 90 °C for 30 min [15,30], and intrinsic a-Si deposition (~50 nm) was used as a reference.

Both, passivation and contact resistivity test samples were subject to $POCl_3$ diffusion processes at 820 °C, 850 °C, and 880 °C. The deposition time (25 min) and the drive-in time (30 min) were kept constant. After diffusion, a subsequent 400 °C forming gas annealing (FGA) for 30 min was performed and the phosphosilicate glass (PSG) was removed by 2% HF solution. In some of our experiments, we have observed degradation in the passivation quality after an HF dip. To minimise the likelihood of such degradation, we perform the HF dip step after the FGA, since we have found that the presence of the PSG has little effect on FGA. For the implied open circuit voltage iV_{oc} measurement, the passivating contact layers were deposited symmetrically on both sides of the wafer. The iV_{oc} values were obtained by Quasi-steady-state photoconductance (QSSPC) under 1-Sun equivalent light intensity [33]. Contact resistivity ρ_c was extracted by the method proposed by Cox and Strack [34]. For the contact resistivity samples, circular aluminium contacts were evaporated on the side with poly-Si passivated contact layers, and full area aluminium was evaporated directly on the c-Si rear side, which was highly doped by phosphorus diffusion. In addition, a photoluminescence (PL) imaging system (BT Imaging LIS-R1, captured at an illumination intensity of 0.5 suns and an exposure time of 0.5s) was used to study the uniformity of the passivation structures before and after the thermal diffusion process. Electrochemical capacitance-voltage (ECV, WEP Wafer Profile CVP21) was used to measure the concentration of electrically active phosphorus dopants in the poly-Si/SiO_xN_y/c-Si structures.

3. Results and discussion

3.1. Uniformity of passivating contacts

We found that the surface passivation quality and uniformity were strongly correlated to the gas flow of the precursors, especially for the SiH_4. In this section, we study the impact of the gas flow on the surface passivation uniformity and post processing stability (i.e. after HF dip) of poly-Si contacts fabricated by this single PECVD process. Fig. 2 shows the photoluminescence images of the samples coated with symmetrical

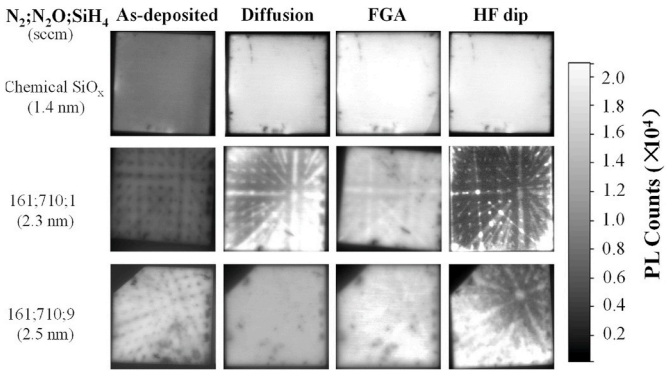

Fig. 2. PL images after different process stages with the SiO_xN_y interfacial layers deposited using different SiH_4 flow (keeping the N_2O and N_2 gas flow constant. The deposition time for 1 and 9 sccm was 30 s and 4s, respectively). A chemical SiO_x sample as a reference is shown. (PL images were captured at an illumination intensity of 0.5 suns and an exposure time of 0.5 s).

SiO_xN_y/a-Si stacks before and after thermal diffusion. Before thermal diffusion, an array of dark spots, corresponding to the locations of the gas outlets in the shower head, was observed in the PL images in all samples with different SiH_4 flows. In contrast, these patterns were not observed in the reference samples with chemical SiO_x layers. After thermal diffusion, these dark spots disappeared for the samples with high SiH_4 flow (9 sccm), while for the samples prepared using a low SiH_4 flow (1 sccm), they became brighter than the surrounding regions. We hypothesise that a low gas flow may result in a non-uniform spatial distribution of SiH_n radicals in the plasma. Interestingly, the subsequent FGA process can improve the uniformity of the passivation. Unfortunately, during the subsequent HF dip process, some silicon flakes floating in the HF solution were observed, indicating poor adhesion between the SiO_xN_y and silicon films. As a result, all samples with different SiH_4 flow rates show poor passivation qualities after HF dip, with a more pronounced degradation for samples with a lower SiH_4 flow (1 sccm). The delamination can be related to material properties such as density and intrinsic stress as well as to interfacial stress originating from the different lattice constants and thermal expansion coefficients [35]. These differences lead to the release of stress during the high-temperature recrystallization process, which eventually resulted in the delamination of the passivation layer during the HF dip.

Nevertheless, we found the poor passivation quality of the poly-Si contacts after HF dip can be effectively improved by reducing the N_2O flow rate, as shown in Fig. 3. The decrease of N_2O flow rate results in a significant increase in the Si content of the film [27]. Thus, less stress is introduced during the recrystallization process [35]. When the N_2O flow rate drops to 50 sccm, the delamination phenomenon is reduced significantly, and no delamination has been observed by decreasing the N_2O gas flow to 20 sccm. We found that the final passivating contact structure has a good structural uniformity when the N_2O flow rate was less than 20 sccm.

Additionally, the influence of N_2 flow on the uniformity of passivating contact structure is also investigated, as shown in Fig. 4. Compared to the impact of SiH_4 flow, Fig. 2, N_2 flow has less effect on the uniformity of SiO_xN_y based poly-Si passivating contact structures. Although in principle N_2 can also provide N during the deposition [36], the extent of N_2 decomposition is limited by the strong N-N bond. The N content in the film is additionally limited by the deposition plasma power. However, increasing N_2 can dilute the reaction gas precursors and therefore affect the deposition rate of the interfacial layer. A higher N_2 flow leads to a lower deposition rate. In order to precisely control the thickness of the SiO_xN_y, we chose 361 sccm as an optimum N_2 flow rate.

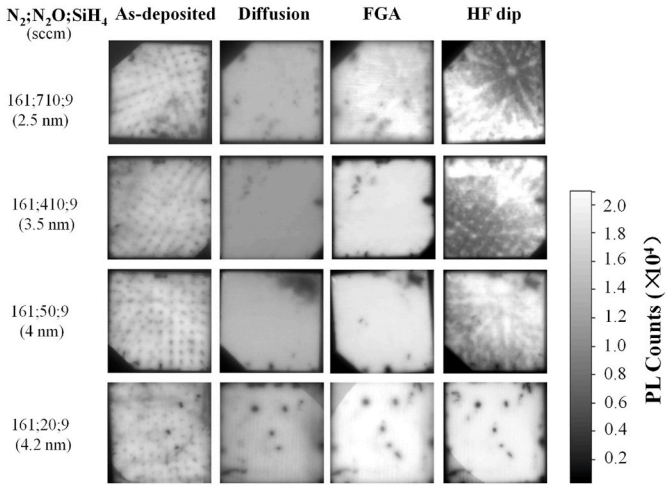

Fig. 3. PL images after different process stages with the SiO_xN_y interfacial layers deposited using different N_2O gas flow (keeping the SiH_4 and N_2 gas flow constant, the deposition time was 4 s). (PL images were captured at an illumination intensity of 0.5 suns and an exposure time of 0.5 s).

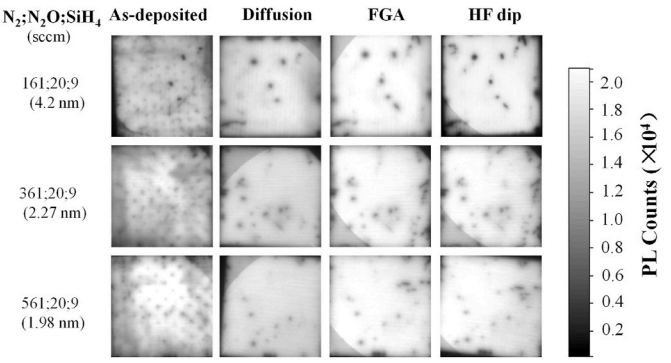

Fig. 4. PL images after different process stages with the SiO_xN_y interfacial layers deposited using different N_2 gas flows. The thickness of the interfacial layer is indicated in brackets. (The deposition time was 4 s, the low PL signal in the corner area is measurement artefact). (PL images were captured at an illumination intensity of 0.5 suns and an exposure time of 0.5 s).

3.2. *Influence of N_2O and SiH_4 flow ratios*

In order to achieve an ultrathin interfacial layer (<3 nm), a short deposition time is required, which may compromise uniformity on large area substrates. In this section we mainly focus on examining the uniformity of the film thickness, as well as the elemental composition of the layers with various gas flows. During the formation of SiO_xN_y films, the plasma reactions mainly contain SiH_n radicals ($n \leq 3$, the number of hydrogen atoms bonded to a single silicon atom), and O and N radicals, which can react to form energetically favourable bonds [27]. Si bonds are essential to form the solid phase, while the O and N can hardly bond to the silicon substrate alone, due to the limited amount of dangling bonds on the surface. Thus, the deposition rate of SiO_xN_y films strongly depends on the number of SiH_n radicals, which provide continuous unsaturated Si bonds. This means that a low flow rate of SiH_4 results in a low SiO_xN_y film deposition rate. The deposition rates were ~4 nm/min for 1 sccm SiH_4, and ~38 nm/min for 9 sccm SiH_4. However, a low SiH_4 flow rate (e.g. 1 sccm) can lead to a significant decrease in SiH_n radicals present in the plasma, resulting in film uniformity issues on large surface areas. Therefore, we investigated the film thickness and refractive index behaviour for SiH_4 flow rates larger than 9 sccm and a fixed N_2 flow rate of 361 sccm. Fig. 5a shows the influence of different N_2O and SiH_4 flow rates on SiO_xN_y thickness and their refractive indices, which were extracted from ellipsometry measurements. The ellipsometry model we used was a Cauchy film on a silicon substrate, with the mean square errors (MSE) of the ellipsometry optical fitting below 2. For a fixed deposition time of 4 s, the thicknesses of the SiO_xN_y layers were within the range of from 2.1 to 2.4 nm. As indicated by the black line in Fig. 5a, the change of N_2O and SiH_4 flow ratio has minor impact on the final layer thickness. On the other hand, the refractive indices (at a wavelength of 633 nm) are strongly dependent on the gas ratios, as indicated by the blue line in Fig. 5a. With decreasing N_2O/SiH_4 ratio, the refractive indices decrease from 2.08 to 1.77, which is still higher than that of chemical SiO_x (a value closes to that of SiO_2, ~1.46). This means that by decreasing the N_2O/SiH_4 ratio, the concentrations of N and Si in the film increase while the concentration of O decreases. As a reference, the value for stoichiometric silicon nitride, Si_3N_4, is ~2.04, and a pure a-Si layer has a refractive index of ~3.88 [37,38].

The contour plot of Fig. 5b shows the film thickness (colour bar) and the refractive index (black numbers) on a 4-inch silicon wafer deposited with gas flow ratio of N_2O:SiH_4 = 25:9. From these results, we find that the PECVD deposition process can obtain good film uniformity in terms of both thickness and refractive index, which have a variation of 10% and 0.5% respectively, in a deposition time as short as 4 s. Nevertheless, the as-deposited film is slightly thicker at the edge of the wafer than in the centre of the wafer, with maximum difference of 0.2 nm.

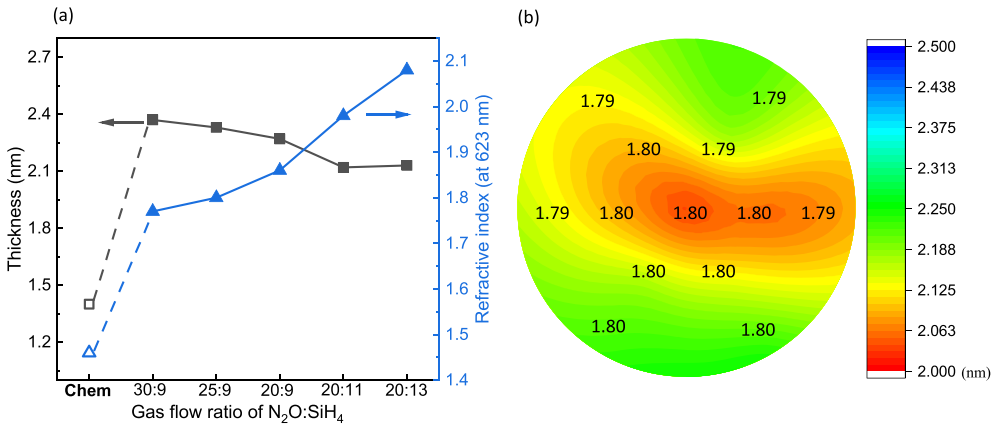

Fig. 5. Thicknesses and refractive indices of different interfacial layers measured by ellipsometry. (a) shows a comparison of SiO_xN_y films deposited with different gas flow rates and chemical SiO_x; (b) shows the uniformity of a film deposited using gas flow ratio of N_2O:SiH_4 = 25:9 on a 4-inch silicon wafer, the thickness variation is shown in the colour scale, while the refractive indices at different locations are indicated by black numbers. (N_2 flow was 361 sccm, the deposition time was 4 s). (For interpretation of the references to colour in this figure legend, the reader is referred to the Web version of this article.)

To further study the elemental composition of the SiN_xO_y films with various gas flow ratio, we performed FTIR studies, as shown in Fig. 6. In order to obtain clear and strong signals, films examined here have a thickness of ~20 nm. The chemical SiO_x is also included here as a reference. Since it is a thin layer with a thickness of ~1.4 nm, only a small Si-O peak around ~1020 cm^{-1} can be observed. As the N_2O/SiH_4 ratio decreases, the ratio of Si-N and Si-O bonds in the film increases significantly. According to the strength of chemical bonds occurring during plasma deposition [39], the most favourable chemical reaction is between SiH_n and O radicals, leading to the formation of Si-O bonds [27]. A precursor molecule disiloxane ($(SiH_3)_2O$) can be formed from the reaction between oxygen atoms and silane, which contains the planar Si-O-Si group that is the structural building block for stoichiometric SiO_2 [40]. A large N_2O/SiH_4 flow ratio leads to an excess of O radicals in comparison with SiH_n radicals, so that the Si-O bonds dominate in the final film. Either by decreasing the gas flow rate of N_2O or decreasing the gas flow rate of SiH_4, SiH_n becomes redundant and starts to combine with N and H radicals, which results in the formation of Si-N and Si-H bonds, even though less N_2O leads to less N radicals [28]. On the other hand, increasing SiH_n radicals can also lead to a high silicon concentration in the film, which results in a silicon rich SiO_xN_y film [28]. This can be confirmed by the Si-H peak shifts in Fig. 6b, which show the Si-H band shifting towards a lower wavenumber with decreasing N_2O or increasing SiH_4 [41]. As the N_2O flow decreases or SiH_4 flow increases, the incorporation of nitrogen and silicon in the form of Si-H, Si-N, N-H and Si-Si becomes more probable, which results in films with higher refractive indices. This is consistent with the ellipsometry measurements in Fig. 5a. In addition, the increment of the Si-H band is also accompanied by a slight decrease in the N-H band (~3377 cm^{-1}), which might be an indication that some N-H bonds are changed to Si-H and Si-N bonds [28,29].

3.3. Impact of the SiO_xN_y films on the doping profiles of poly-Si contacts

The doping profile, which is strongly affected by the interfacial layer, is essential to achieve high performing poly-Si passivating contacts [21,42,43]. Fig. 7 shows the doping profiles (measured by ECV) of poly-Si contacts based on PECVD SiO_xN_y (using a fixed N_2 flow of 361 sccm) with different gas flow ratios. A constant phosphorous doping of 3×10^{20} cm^{-3} is observed in the poly-Si layer for all samples, including the reference sample with the chemical SiO_x. It is interesting to note that the doping levels within the silicon substrates are different for samples with the various SiO_xN_y layers. The shallowest doping depth is found in the samples with chemical SiO_x and SiO_xN_y with N_2O:SiH_4 = 30:9. The sheet resistance values (R_{sh}) extracted from conductance measurements decrease with either increasing SiH_4 or decreasing N_2O flows. The lowest R_{sh} of 26.2 Ω/□ was obtained for N_2O:SiH_4 flow ratio of 20:13 (with a thickness of 2.13 nm and refractive index of 2.08) and the highest R_{sh} of 59.7 Ω/□ was obtained for the sample with gas flow ratio of 30:9 (with a thickness of 2.37 nm and refractive index of 1.77). Compared to the sample with the nitric oxide (R_{sh} = 72.6 Ω/□), we conclude that the thin chemical SiO_x (~ 1.4 nm) forms a stronger barrier for phosphorus diffusion. This may be due to: 1) the chemical SiO_x layer is denser than PECVD SiO_xN_y film; 2) phosphorus has a different diffusivity in different dielectric films. It has been shown previously that a silicon rich film can enhance the diffusivity of phosphorus and cause

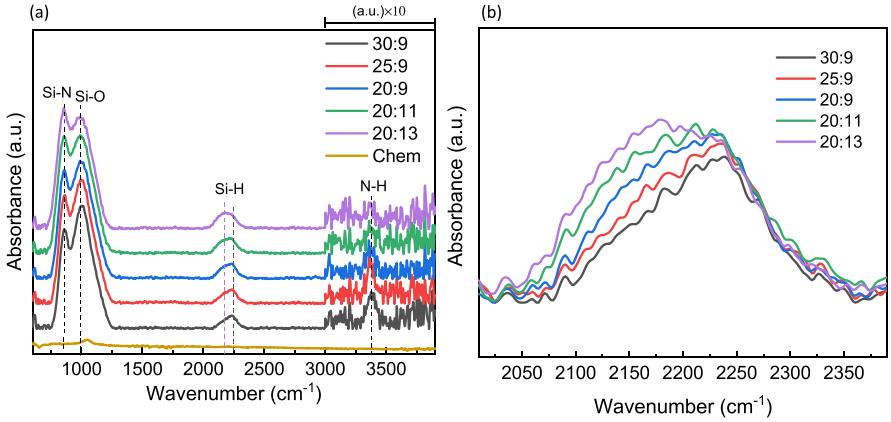

Fig. 6. FTIR spectra of ~20 nm as-deposited SiO_xN_y layers for different gas flow ratios, and a ~1.4 nm chemical SiO_x layer as a reference shown by the yellow line in (a); with a detailed view of the Si-H peak in (b). (For interpretation of the references to colour in this figure legend, the reader is referred to the Web version of this article.)

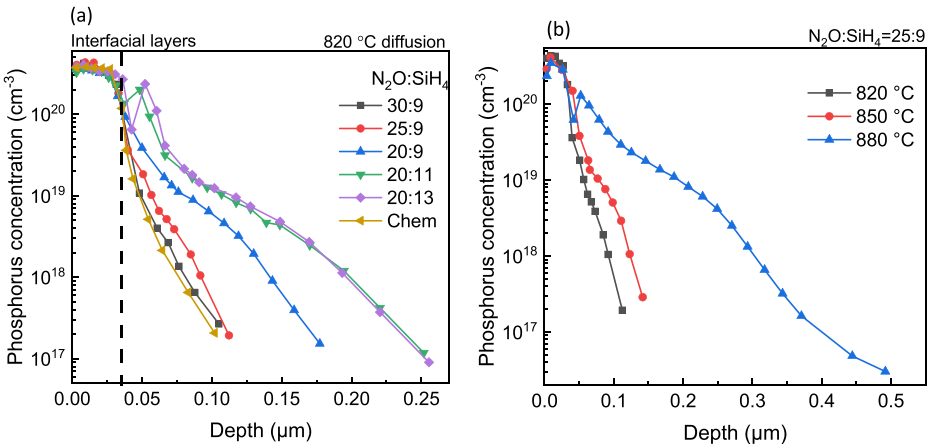

Fig. 7. ECV doping profiles for samples with interfacial SiO_xN_y layers of different gas flow rates and chemical SiO_x as reference after a 820 °C diffusion (a), and for the SiO_xN_y layers of N_2O:SiH_4 = 25:9 gas flow ratio varying the diffusion temperature (b).

higher doping concentrations in the silicon substrate [44]. In addition, studies [21,42] have shown that adding N atoms to the interfacial layer is beneficial to reduce the penetration of dopants. Based on the measured refractive indices and FTIR results, the SiH_4 flow rates of 11 and 13 sccm (n = 1.98 & 2.08) can result in Si rich SiO_xN_y films. In addition, a shallower doping profile (high R_{sh}) is obtained in the poly-Si contact structure with high N_2O gas flow. This might be due to the changes in the ratio of Si-N, Si-O, Si-H and N-H bonds in SiO_xN_y layers, as discussed in relation to the FTIR results. Our experimental results indicate that the effect of increasing the Si content (increasing penetration of phosphorus) is more dominant than that of increasing the N content (decreasing penetration of phosphorus) within our tested gas flow range.

The doping concentration of the sample with N_2O:SiH_4 = 25:9 flow ratio was further studied as a function of diffusion temperatures, as shown in Fig. 7b. Consequently, the R_{sh} decreased from 49.2 Ω/□ at 820 °C to 19.8 Ω/□ at 880 °C. When the diffusion temperature reaches 880 °C, the interfacial layer is no longer a good diffusion barrier for phosphorus atoms. We suspect that a large degree of film break-up has occurred at this temperature, similar to the break-up phenomenon observed in chemical silicon oxide [45]. For chemical SiO_x samples, the R_{sh} decreased from 76.2 Ω/□ at 820 °C to 11.8 Ω/□ at 880 °C, showing a greater drop than the sample using SiO_xN_y as the interfacial layer. This seems to show that SiO_xN_y has a smaller degree of break-up with increasing temperature than SiO_x, which may be due to the thicker layers, or the addition of N.

3.4. Performance of passivating contacts with different SiO_xN_y layers

Fig. 8 shows the electrical performance, iV_{oc} and ρ_c, of poly-Si passivating contacts with five different SiO_xN_y interlayers, as discussed in section 3.3. The iV_{oc} values of a-Si/SiO_xN_y/c-Si before and after 820 °C diffusion are shown as a function of the N_2O:SiH_4 gas flow ratios (N_2 flow rate is fixed at 361 sccm), as indicated by solid lines in Fig. 8a. For as-deposited structures (before thermal diffusion), the passivation qualities of SiO_xN_y samples are higher than that of the reference sample with chemical SiO_x. This is mainly because the as-deposited SiO_xN_y film contains higher hydrogen concentration (shown in the FTIR result in Fig. 6) that is able to provide good surface passivation, which has also been reported in other works [46,47]. We suspect that since the SiO_xN_y films used in these samples is a silicon rich layer with refractive indices ≥1.77, the performance before and after high temperature treatments is similar to the a-Si:H case. With either decreasing N_2O flow or increasing SiH_4 flow, films with higher hydrogen and Si concentrations are achieved, which results in high surface passivation quality, a higher iV_{oc}. After the high temperature thermal diffusion and a subsequent FGA process, the highest iV_{oc} value of 711 mV is achieved for the sample with N_2O:SiH_4 = 25:9. In fact, the sample with this interfacial layer also has a shallow substrate doping profile, as shown in Fig. 7a. However, the 30:9 sample with the shallowest doping profile has a slightly lower iV_{oc} of 698 mV. Two factors may be responsible for the slight decline in iV_{oc}: 1) The change of gas flow ratio can lead to a change of chemical composition in SiO_xN_y, as shown in Fig. 6, thus affecting the band gap of SiO_xN_y [25], and therefore carrier tunneling across the interface. 2) A lower N content results in a lower

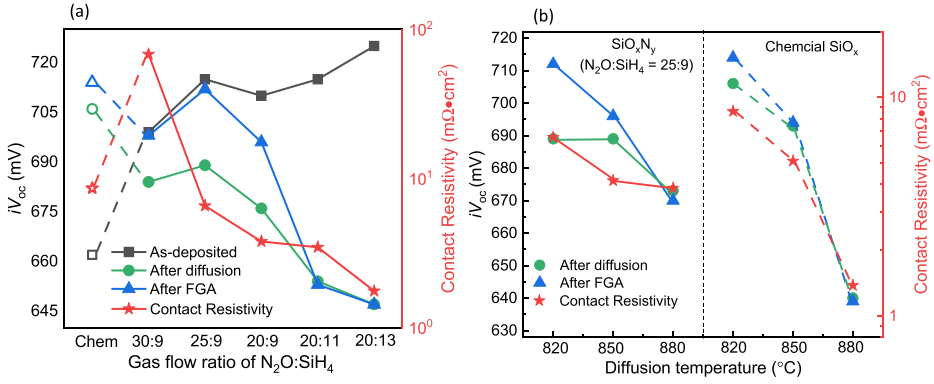

Fig. 8. Implied open circuit voltage and contact resistivity of final passivating contact structures. (a) SiO_xN_y layers of different gas flow ratios and chemical SiO_x as reference with a 820 °C diffusion temperature ; (b) SiO_xN_y layers with a 25:9 gas flow ratio (N_2O:SiH_4) varying the diffusion temperature. (The thicknesses of SiO_xN_y are shown in Fig. 2a).

dielectric constant, yielding a lower positive fixed charge [48], resulting in a decrease in field-effect passivation. On the other hand, a very low iV_{oc} value, < 650 mV, is obtained for the two samples with higher SiH_4 flow rates (11 and 13 sccm). These have quite deep doping depths in the silicon substrate and their passivation qualities were not further improved by the subsequent FGA process. Regarding the subsequent FGA process, the iV_{oc} of the 30:9, 25:9 and 20:9 samples improved significantly (from 684 mV to 698 mV, 689 mV–712 mV and 676 mV–696 mV, respectively). Based on the results shown in Fig. 7a, less phosphorus penetration (low doping at the interface between the silicon substrate and the SiO_xN_y layers), and a lower extent of interfacial layer break-up (low diffusion temperatures), have stronger responses to the FGA process. Both the phosphorus penetration and the extent of interfacial layer break-up are strongly dependent on the elemental composition of the SiO_xN_y interfacial layers, as discussed in Section 3.2. In addition, FGA was found to improve the iV_{oc} of SiO_xN_y samples more than that of the chemical SiO_x sample. This might point to a higher amount of interfacial defects in the PECVD SiO_xN_y interfacial layers compared to the chemical SiO_x, which might originate from ion bombardment during plasma deposition. Another reason might be that chemical SiO_x has a larger bandgap resulting in a stronger band bending, making it less sensitive to FGA. In terms of their contact resistivity values, as indicated by a red line in Fig. 8a, the contact resistivity ρ_c decreases from 68.2 mΩ cm^2 (30:9) down to 1.8 mΩ cm^2 (20:13). This could be due to the deeper penetration of phosphorus into the substrate. The ECV result of the sample with $N_2O:SiH_4 = 30:9$ is similar to that of the chemical SiO_x samples, but shows a significantly higher contact resistivity. This indicates that the carrier selectivity of such passivating contact structures can also be affected by the N concentration in the interfacial layers. High N content may result in a higher contact resistivity. In addition, the thicker layer of SiO_xN_y (2.37 nm) than that of SiO_x (1.4 nm) may also lead to a higher contact resistivity. Based on the results of iV_{oc} (711 mV) and contact resistivity ρ_c (6.6 mΩ cm^2), the optimal SiO_xN_y deposition is achieved with gas flow rates of $N_2O = 25$ sccm, $SiH_4 = 9$ sccm and $N_2 = 361$ sccm.

In addition, the electrical performance of samples with $N_2O:SiH_4 = 25:9$ is further examined as a function of diffusion temperature in comparison with chemical SiO_x samples, as shown in Fig. 8b. With increasing diffusion temperature, iV_{oc} decreases, and the response to FGA becomes weaker for both SiO_xN_y and chemical SiO_x samples. We attribute this behaviour to a higher break-up/pinhole density at higher diffusion temperature. As shown in Fig. 7b, when the diffusion temperature reaches 880 °C, the interfacial layer no longer acts as a good diffusion barrier for phosphorus, indicating a high density of SiO_xN_y break-up. However, at this high diffusion temperature of 880 °C, the iV_{oc} of the SiO_xN_y sample reaches 670 mV, while a lower iV_{oc} of 640 mV is observed for the chemical SiO_x sample. On the other hand, the lowest contact resistivity of SiO_xN_y samples is almost three times higher than that of chemical SiO_x samples (1.32 mΩ cm^2 at 880 °C for chemical SiO_x samples and 3.8 mΩ cm^2 at 820 °C for SiO_xN_y samples). With the increase of diffusion temperature, the deterioration of passivation quality and the decrease of contact resistivity of SiO_xN_y samples is less pronounced than those of the chemical SiO_x. This might be mainly because the SiO_xN_y layer is thicker than the chemical SiO_x layer and it may benefit from variations in the chemical composition of the interfacial layer, e.g. the addition of N. Finally, an optimal iV_{oc} of ~711 mV in combination with a contact resistivity of ~6.6 mΩ cm^2 was achieved for the passivating contact structure with a SiO_xN_y layer, which is close to values obtained using the chemical SiO_x. Note that due to a suboptimal a-Si deposition process, an overall lower performance was achieved in the sample series presented here compared to our earlier work with iV_{oc} performance of >740 mV using a similar process with chemical SiO_x, as shown in Ref. [49].

4. Conclusion

In order to simplify the fabrication of poly-Si passivating contact structures, reduce the potential contamination risk during transferring processes, and allow variations to the film composition, we have developed a simple PECVD deposition process that combines the deposition of SiO_xN_y interfacial film and amorphous silicon films, achieving excellent electrical performance.

We found that increasing the SiH_4 flow rate from 1 sccm to 9 sccm can significantly improve the films structural stability. Additionally, reducing the $N_2O:SiH_4$ gas flow ratio can reduce the stress between the films, which makes the poly-Si contact structure more stable during subsequent chemical processes, e.g. HF dip. For a precise control of the thickness of such thin interfacial layers, a higher N_2 flow is beneficial as it lowers the deposition rate. We found that a chemically stable and uniform passivating contact can be achieved by using gas flow ratio of $N_2:N_2O:SiH_4 = 361:25:9$. After phosphorus diffusion and FGA, a high iV_{oc} value of 711 mV with a contact resistivity of ~6.6 mΩ cm^2 was realized. It is expected that by further optimising the intrinsic a-Si deposition process, the diffusion condition and the hydrogenation step, excellent SiO_xN_y based poly-Si contacts can be achieved.

CRediT authorship contribution statement

Wenhao Chen: Conceptualization, Methodology, Validation, Data curation, Writing – original draft. **Josua Stuckelberger:** Data curation, Writing – review & editing. **Wenjie Wang:** Investigation. **Sieu Pheng Phang:** Writing – review & editing. **Daniel Macdonald:** Supervision, Validation, Funding acquisition. **Yimao Wan:** Writing – review & editing, Funding acquisition. **Di Yan:** Resources, Writing – review & editing, Project administration.

Declaration of competing interest

The authors declare that they have no known competing financial interests or personal relationships that could have appeared to influence the work reported in this paper.

Acknowledgements

This work has been supported by the Australian Renewable Energy Agency (ARENA) via the Australian Centre for Advanced Photovoltaics (ACAP), and by the National Key R&D Program of China 2018YFB1500503. Facilities at the Australian National Fabrication Facility were used for the film deposition and thickness measurements. The authors would like to thank the Department of Electronic Materials Engineering at ANU, for providing access to the FTIR equipment.

References

[1] H. De Graaff, J.G. De Groot, The SIS tunnel emitter: a theory for emitters with thin interface layers, IEEE Trans. Electron. Dev. 26 (1979) 1771–1776.
[2] J. Graul, A. Glasl, H. Murrmann, High-performance transistors with arsenic-implanted polysil emitters, IEEE J. Solid State Circ. 11 (1976) 491–495.
[3] Y.H. Kwark, R. Sinton, R.M. Swanson, SIPOS Heterojunction Contacts to Silicon, 1984 International Electron Devices Meeting, IEEE, 1984, pp. 742–745.
[4] Y. Kwark, R. Sinton, R. Swanson, Low J° contact structures using sipos and polysilicon films, IEEE Photovolt. Specialists Conf. 18 (1985) 787–791.
[5] J.-Y. Gan, R. Swanson, Polysilicon emitters for silicon concentrator solar cells, in: IEEE Conference on Photovoltaic Specialists, IEEE, 1990, pp. 245–250.
[6] A. Richter, R. Müller, J. Benick, F. Feldmann, S.W. Glunz, Design rules for high-efficiency both-sides-contacted silicon solar cells with balanced charge carrier transport and recombination losses, Nat. Energy 6 (2021).
[7] F. Haase, C. Hollemann, S. Schäfer, A. Merkle, M. Rienäcker, J. Krügener, R. Brendel, R. Peibst, Laser contact openings for local poly-Si-metal contacts enabling 26.1%-efficient POLO-IBC solar cells, Sol. Energy Mater. Sol. Cell. 186 (2018) 184–193.
[8] G.L. Patton, J.C. Bravman, J.D. Plummer, Physics, technology, and modeling of polysilicon emitter contacts for VLSI bipolar transistors, IEEE Trans. Electron. Dev. 33 (1986) 1754–1768.

[9] P.A. Potyraj, D.-L. Chen, M.K. Hatalis, D.W. Greve, Interfacial oxide, grain size, and hydrogen passivation effects on polysilicon emitter transistors, IEEE Trans. Electron. Dev. 35 (1988) 1334–1343.

[10] T.G. Allen, J. Bullock, X. Yang, A. Javey, S. De Wolf, Passivating Contacts for Crystalline Silicon Solar Cells, Nature Energy, 2019, pp. 1–15.

[11] J. Schmidt, R. Peibst, R. Brendel, Surface passivation of crystalline silicon solar cells: present and future, Sol. Energy Mater. Sol. Cell. 187 (2018) 39–54.

[12] M. Hermle, F. Feldmann, M. Bivour, J.C. Goldschmidt, S.W. Glunz, Passivating contacts and tandem concepts: approaches for the highest silicon-based solar cell efficiencies, Appl. Phys. Rev. 7 (2020), 021305.

[13] U. Römer, R. Peibst, T. Ohrdes, B. Lim, J. Krügener, E. Bugiel, T. Wietler, R. Brendel, Recombination behavior and contact resistance of n+ and p+ poly-crystalline Si/mono-crystalline Si junctions, Sol. Energy Mater. Sol. Cell. 131 (2014) 85–91.

[14] F. Feldmann, M. Bivour, C. Reichel, M. Hermle, S.W. Glunz, Passivated rear contacts for high-efficiency n-type Si solar cells providing high interface passivation quality and excellent transport characteristics, Sol. Energy Mater. Sol. Cell. 120 (2014) 270–274.

[15] H. Kobayashi Asuha, O. Maida, M. Takahashi, H. Iwasa, Nitric acid oxidation of Si to form ultrathin silicon dioxide layers with a low leakage current density, J. Appl. Phys. 94 (2003) 7328–7335.

[16] R. van der Vossen, F. Feldmann, A. Moldovan, M. Hermle, Comparative study of differently grown tunnel oxides for p-type passivating contacts, Energy Procedia 124 (2017) 448–454.

[17] D. Yan, A. Cuevas, J. Bullock, Y. Wan, C. Samundsett, Phosphorus-diffused polysilicon contacts for solar cells, Sol. Energy Mater. Sol. Cell. 142 (2015) 75–82.

[18] A. Moldovan, F. Feldmann, K. Kaufmann, S. Richter, M. Hermle, Tunnel Oxide Passivated Carrier-Selective Contacts Based on Ultra-thin SiO2 Layers Grown by Photo-Oxidation or Wet-Chemical Oxidation in Ozonized Water, Photovoltaic Specialist Conference, 2015.

[19] A. Moldovan, F. Feldmann, G. Krugel, M. Zimmer, J. Rentsch, M. Hermle, A. Roth-Fölsch, K. Kaufmann, C. Hagendorf, Simple cleaning and conditioning of silicon surfaces with UV/ozone sources, Energy Procedia 55 (2014) 834–844.

[20] Y. Huang, M. Liao, Z. Wang, X. Guo, C. Jiang, Q. Yang, Z. Yuan, D. Huang, J. Yang, X. Zhang, Ultrathin silicon oxide prepared by in-line plasma-assisted N2O oxidation (PANO) and the application for n-type polysilicon passivated contact, Sol. Energy Mater. Sol. Cell. 208 (2020), 110389.

[21] F. Feldmann, J. Schoen, J. Niess, W. Lerch, M. Hermle, Studying dopant diffusion from poly-Si passivating contacts, Sol. Energy Mater. Sol. Cell. 200 (2019), 109978.

[22] D. Shubham, N. Naomi, P. Pradeep, B.J. Kitz, S. Rolf, A.G. Aberle, monoPoly cells: large-area crystalline silicon solar cells with fire-through screen printed contact to doped polysilicon surfaces, Sol. Energy Mater. Sol. Cell. 187 (2018) 76–81.

[23] N. Naomi, R. John, K. Thomas, G. Thomas, F. Lauretta, P. Pradeep, B. Nagarajan, K. Marcel, D. Shubham, Approaching 23% with large-area monoPoly cells using screen-printed and fired rear passivating contacts fabricated by inline PECVD, Prog. Photovoltaics Res. Appl. (2019) 27.

[24] M. Stöhr, J. Aprojanz, R. Brendel, T. Dullweber, Firing-stable PECVD SiO x N y/n-Poly-Si surface passivation for silicon solar cells, ACS Appl. Energy Mater. 4 (2021) 4646–4653.

[25] F. Rebib, E. Tomasella, J.P. Gaston, C. Eypert, J. Cellier, M. Jacquet, Determination of optical properties of a-SiOxNy thin films by ellipsometric and UV-visible spectroscopies, J. Phys. Conf. 100 (2008), 082033.

[26] R. Peibst, U. Römer, Y. Larionova, M. Rienäcker, A. Merkle, N. Folchert, S. Reiter, M. Turcu, B. Min, J. Krügener, D. Tetzlaff, E. Bugiel, T. Wietler, R. Brendel, Working principle of carrier selective poly-Si/c-Si junctions: is tunnelling the whole story? Sol. Energy Mater. Sol. Cell. 158 (2016) 60–67.

[27] M. Hussein, K. Wörhoff, G. Sengo, A. Driessen, Optimization of plasma-enhanced chemical vapor deposition silicon oxynitride layers for integrated optics applications, Thin Solid Films 515 (2007) 3779–3786.

[28] M. Alayo, I. Pereyra, W. Scopel, M.d.A. Fantini, On the nitrogen and oxygen incorporation in plasma-enhanced chemical vapor deposition (PECVD) SiOxNy films, Thin Solid Films 402 (2002) 154–161.

[29] R. Pandey, L. Patil, J. Bange, D. Patil, A. Mahajan, D. Patil, D. Gautam, Growth and characterization of SiON thin films by using thermal-CVD machine, Opt. Mater. 25 (2004) 1–7.

[30] Asuha, T. Kobayashi, O. Maida, M. Inoue, M. Takahashi, Y. Todokoro, H. Kobayashi, Ultrathin silicon dioxide layers with a low leakage current density formed by chemical oxidation of Si, Appl. Phys. Lett. 81 (2002) 3410–3412.

[31] W. Chen, T.N. Truong, H.T. Nguyen, C. Samundsett, S.P. Phang, D. MacDonald, A. Cuevas, L. Zhou, Y. Wan, D. Yan, Influence of PECVD deposition temperature on phosphorus doped poly-silicon passivating contacts, Sol. Energy Mater. Sol. Cell. (2020) 206.

[32] W. Chen, J. Stuckelberger, W. Wang, S.P. Phang, D. Kang, C. Samundsett, D. MacDonald, A. Cuevas, L. Zhou, Y. Wan, Influence of PECVD deposition power and pressure on phosphorus-doped polysilicon passivating contacts, IEEE J. Photovolt. 10 (2020) 1239–1245.

[33] D. Kane, R. Swanson, Measurement of the emitter saturation current by a contactless photoconductivity decay method, IEEE Photovolt. Specialists Conf. 18 (1985) 578–583.

[34] R. Cox, H. Strack, Ohmic contacts for GaAs devices, Solid State Electron. 10 (1967) 1213–1218.

[35] M. Carreno, M. Alayo, I. Pereyra, A. Lopes, PECVD-SiOxNy films for large area self-sustained grids applications, Sensor Actuator Phys. 100 (2002) 295–300.

[36] D. Criado, I. Pereyra, M. Alayo, Study of nitrogen-rich silicon oxynitride films obtained by PECVD, Mater. Char. 50 (2003) 167–171.

[37] G. Tsutsumanova, A. Tzonev, S. Russev, Polynomial inversion of the single transparent layer problem in ellipsometry in case of multiple measurements, Phys. Status Solidi C 5 (2008) 1054–1058.

[38] P. Heimala, J. Aarnio, Refractive index behaviour of phosphorus-doped planar silica waveguides, J. Phys. Appl. Phys. 25 (1992) 733.

[39] D.R. Lide, CRC Handbook of Chemistry and Physics, CRC press, 2004.

[40] G. Lucovsky, Deposition of silicon dioxide and silicon nitride by remote plasma enhanced chemical vapor deposition, J. Vac. Sci. Technol.: Vacuum, Surf. Films 4 (1986) 681–688.

[41] V. Tomar, D. Patil, D. Gautam, Deposition and characterization of SiON films using HMDS for photonics applications, Semicond. Sci. Technol. 22 (2006) 43.

[42] D. Yan, A. Cuevas, Y. Wan, J. Bullock, Silicon nitride/silicon oxide interlayers for solar cell passivating contacts based on PECVD amorphous silicon, Phys. Status Solidi Rapid Res. Lett. 9 (2015) 617–621.

[43] D. Yan, A. Cuevas, Y. Wan, J. Bullock, Passivating contacts for silicon solar cells based on boron-diffused recrystallized amorphous silicon and thin dielectric interlayers, Sol. Energy Mater. Sol. Cell. 152 (2016) 73–79.

[44] K. Sakamoto, K. Nishi, F. Ichikawa, S. Ushio, Segregation and transport coefficients of impurities at the Si/SiO2 interface, J. Appl. Phys. 61 (1987) 1553–1555.

[45] F. Feldmann, G. Nogay, J.-I. Polzin, B. Steinhauser, A. Richter, A. Fell, C. Schmiga, M. Hermle, S.W. Glunz, A study on the charge carrier transport of passivating contacts, IEEE J. Photovolt. 8 (2018) 1503–1509.

[46] C. Seager, D. Ginley, Passivation of grain boundaries in polycrystalline silicon, Appl. Phys. Lett. 34 (1979) 337–340.

[47] B. Hallam, B. Tjahjono, S. Wenham, Effect of PECVD silicon oxynitride film composition on the surface passivation of silicon wafers, Sol. Energy Mater. Sol. Cell. 96 (2012) 173–179.

[48] Y. Ma, T. Yasuda, G. Lucovsky, Fixed and trapped charges at oxide–nitride–oxide heterostructure interfaces formed by remote plasma enhanced chemical vapor deposition, J. Vac. Sci. Technol. B: Microelectron. Nanometer Struct. Process., Measur. Phenomena 11 (1993) 1533–1540.

[49] W. Chen, T.N. Truong, H.T. Nguyen, C. Samundsett, S.P. Phang, D. MacDonald, A. Cuevas, L. Zhou, Y. Wan, D. Yan, Influence of PECVD deposition temperature on phosphorus doped poly-silicon passivating contacts, Sol. Energy Mater. Sol. Cell. 206 (2020), 110348.